



HHS Public Access

Author manuscript

Neuroimage. Author manuscript; available in PMC 2017 December 01.

Published in final edited form as:

Neuroimage. 2016 December ; 143: 267–279. doi:10.1016/j.neuroimage.2016.09.015.

Functional Magnetic Resonance Imaging of the Cervical Spinal Cord During Thermal Stimulation Across Consecutive Runs

Kenneth A. Weber II^{a,*}, Yufen Chen^a, Xue Wang^a, Thorsten Kahnt^b, and Todd B. Parrish^a

^aDepartment of Radiology, Northwestern University, 737 North Michigan Avenue, Suite 1600, Chicago, IL 60611, USA

^bDepartment of Neurology, Northwestern University, 303 East Chicago Avenue, Ward 13-006, Chicago, IL 60611, USA

Abstract

The spinal cord is the first site of nociceptive processing in the central nervous system and has a role in the development and perpetuation of clinical pain states. Advancements in functional magnetic resonance imaging are providing a means to non-invasively measure spinal cord function, and functional magnetic resonance imaging may provide an objective method to study spinal cord nociceptive processing in humans. In this study, we tested the validity and reliability of functional magnetic resonance imaging using a selective field-of-view gradient-echo echo-planar-imaging sequence to detect activity induced blood oxygenation level-dependent signal changes in the cervical spinal cord of healthy volunteers during warm and painful thermal stimulation across consecutive runs. At the group and subject level, the activity was localized more to the dorsal hemicord, the spatial extent and magnitude of the activity was greater for the painful stimulus than the warm stimulus, and the spatial extent and magnitude of the activity exceeded that of a control analysis. Furthermore, the spatial extent of the activity for the painful stimuli increased across the runs likely reflecting sensitization. Overall, the spatial localization of the activity varied considerably across the runs, but despite this variability, a machine-learning algorithm was able to successfully decode the stimuli in the spinal cord based on the distributed pattern of the activity. In conclusion, we were able to successfully detect and characterize cervical spinal cord activity during thermal stimulation at the group and subject level.

Keywords

Humans; Functional MRI; Spinal Cord; Cervical Cord; Sensory Function; Pain; Upper Extremity

* **Corresponding Author.** Kenneth A. Weber II, DC, PhD. Interdepartmental Neuroscience Program. Department of Radiology. Northwestern University. 737 North Michigan Avenue Suite 1600. Chicago, IL 60611. +1 847-997-6299 (Mobile). +1 312-695-1626 (Work). kweber@u.northwestern.edu.

Publisher's Disclaimer: This is a PDF file of an unedited manuscript that has been accepted for publication. As a service to our customers we are providing this early version of the manuscript. The manuscript will undergo copyediting, typesetting, and review of the resulting proof before it is published in its final citable form. Please note that during the production process errors may be discovered which could affect the content, and all legal disclaimers that apply to the journal pertain.

1. Introduction

The central processing of nociceptive information begins in the spinal cord (SC) (Green, 2004; Willis and Westlund, 1997). Through animal studies, we have gained extensive knowledge about SC nociceptive processing including the central projections of primary afferents (Light and Perl, 1979; Sugiura et al., 1986), the SC circuitry that integrates and relays nociceptive signals to other central targets (Apkarian and Hodge, 1989; Willis et al., 1979), and the descending supraspinal control systems that modulate nociceptive processing in the SC (Carstens et al., 1979; Lin et al., 1994). This knowledge has provided the neurophysiological grounds for many clinical pain phenomena (e.g., hyperalgesia, allodynia, referred pain, etc.) and new targets for treatment (Latremoliere and Woolf, 2009). Overall, animal studies have expanded our understanding of the SC pathophysiology in clinical pain states; however, there are limitations in the ability to translate animal research findings to humans (Hackam and Redelmeier, 2006; van der Worp et al., 2010), and an objective method to study SC nociceptive processing in humans would allow for the direct study of the SC pathophysiology in clinical pain states and advance clinical pain research.

A major advancement in pain research has been the application of functional magnetic resonance imaging (fMRI), allowing for the non-invasive, high-spatial resolution mapping of pain-related neural activity. fMRI research has enhanced our understanding of supraspinal nociceptive processing, pain perception, clinical pain states, and the functional changes in the brain underlying the transition from acute to chronic pain (Apkarian et al., 2005; Mansour et al., 2014). Furthermore, the non-invasiveness of fMRI makes it well suited for longitudinal pain research, and the ability to use fMRI in both animal and human studies supports the forward translation of animal findings to clinical research and the reverse translation of clinical findings to animal models (Mao, 2009).

Over the last two decades, a growing base of researchers have been developing increasingly sophisticated methods for SC fMRI, and the means to objectively measure SC nociceptive processing in humans has become more and more practical (for review see (Kolesar et al., 2015; Stroman et al., 2014; Wheeler-Kingshott et al., 2014)). To date, several independent groups have used fMRI to study SC processing in both animals and humans using thermal (Brooks et al., 2012; Cadotte et al., 2012; Cahill and Stroman, 2011; Khan and Stroman, 2015; Nash et al., 2013; Summers et al., 2010; Yang et al., 2015), chemical (Malisza and Stroman, 2002; Porszasz et al., 1997), and electrical (Endo et al., 2008; Lilja et al., 2006; Zhao et al., 2009) experimental pain paradigms. Moreover, some studies have even demonstrated supraspinal influences on SC nociceptive processing (Dobek et al., 2014; Eippert et al., 2009; Geuter and Buchel, 2013; Sprenger et al., 2012).

The purpose of this study was to test the validity of fMRI using a selective field-of-view gradient-echo echo-planar-imaging sequence to detect activity induced blood oxygenation level-dependent (BOLD) signal changes in the SC during warm and painful thermal stimulation. We hypothesized that the SC activity to thermal stimuli would be anatomically specific (located primarily to the ipsilateral dorsal quadrant of the SC), proportional to the stimulus temperature, and exceed a control analysis at both the group and subject level. Furthermore, because the reliability of the SC fMRI signal during noxious thermal

stimulation needs to be further assessed (Kolesar et al., 2015), we also evaluated the reliability of the signal across consecutive runs. Finally, in order to quantify the amount of pain-related information present in the SC, we utilized a machine-learning algorithm to decode the thermal stimuli based on the distributed patterns of SC activity.

2. Methods

2.1 Participants

Twelve healthy volunteers (9 male and 3 female; average age \pm one standard deviation (SD) 28.8 ± 2.5 years) were studied. Subjects reported no significant pain, neuromusculoskeletal diseases, or contraindications to MRI. The subjects were informed that the study aimed to investigate pain processing using thermal stimulation and fMRI. The entire study protocol was explained to the subjects, and the subjects provided written informed consent. Northwestern University's Institutional Review Board approved this study.

2.2 Imaging protocol

Imaging was performed with a 3.0 Tesla Siemens Prisma (Erlangen, Germany) magnetic resonance (MR) scanner equipped with a 64-channel head/neck coil. Head coil elements 1–4 were turned off during imaging to minimize motion and flow artifacts from the internal carotid arteries. Head coil elements 5–7 (inferior portion of the head coil) and neck coil elements anterior and posterior (24 channels total) were used to capture the MR signal. To increase the magnetic field homogeneity across the cervical spine and to reduce bulk motion during scanning, a SatPad™ cervical collar was used (Maehara et al., 2014). For the functional images, thirty-one transverse slices of the cervical SC were acquired with a T_2^* -weighted gradient-echo echo-planar-imaging sequence using ZOOMit selective field-of-view imaging (TR = 2500 ms, TE = 30 ms, flip angle = 80° , acquisition matrix = 128×44 , field-of-view = 128×44 mm², in-plane resolution = 1×1 mm², slice thickness = 3 mm) (Pfeuffer et al., 2002; Rieseberg et al., 2002). The imaged volume spanned from the superior endplate of the third cervical vertebra to the superior endplate of the first thoracic vertebra (Figure 1). For registration of the functional images to template space, a high-resolution T_2 -weighted structural image of the entire cervical spine and upper thoracic spine was acquired using a single slab three-dimensional turbo spin echo sequence with a slab selective, variable excitation pulse (SPACE, TR = 1500 ms, TE_{eff} = 115 ms, echo train length = 78, flip angle = $90^\circ/140^\circ$, effective resolution = $0.8 \times 0.8 \times 0.8$ mm³, interpolated resolution = $0.8 \times 0.4 \times 0.4$ mm³) (Lichy et al., 2005; Mugler et al., 2000). The imaging protocol was the same as used in our previous study exploring SC activity during an upper extremity motor task (Weber et al., 2016).

2.3 Thermal stimulation protocol

Prior to scanning and outside of the scanner room, subjects were familiarized to the thermal stimulation protocol, and pain threshold temperatures and temperature-pain response functions were calculated. Thermal stimuli were applied to the lateral aspect of the ventral proximal right forearm (Advanced Thermal Stimulator with fMRI filter, 900 mm² square activation area, Pathway Pain and Sensory Evaluation System, Medoc Ltd., Ramat Yishai, Israel). To familiarize subjects, a range of thermal stimuli were applied in 1.0°C increments

from 43.0°C up to 50.0°C as tolerated. For each stimulus, the thermode temperature was increased from a baseline temperature of 30.0°C at a rate of 5.0°C/s to the destination temperature, held for a duration of 7.5 s, and then decreased at a rate of 5.0°C/s back to a baseline temperature of 30.0°C. After each stimulus, the subjects were asked to practice rating their pain experience using a 101-point verbal numerical rating scale (NRS) with anchors of “no pain” (0) and “worst imaginable pain” (100) (Hawker et al., 2011).

For the pain threshold temperatures, the thermode temperature was increased from a baseline temperature of 30.0°C at a rate of 0.5°C/s. When the sensory experience changed from warmth to pain, the subjects were instructed to press a button, and then the thermode temperature returned to baseline at a rate of 5.0°C/s. The temperature at the time of the button press was recorded, the procedure was repeated an additional three times, and the last three temperatures were averaged to determine the pain threshold temperature.

Temperature-pain response functions were then calculated. Thermal stimuli were applied with destination temperatures in 1.0°C increments from the pain threshold temperature – 1.0°C up to the pain threshold temperature + 4.0°C as tolerated (baseline temperature = 30.0°C, destination rate = 5.0°C/s, duration = 7.5 s, return rate 5.0°C/s). Two thermal stimuli at each destination temperature were applied, and the order of the thermal stimuli was randomized. Following each stimulus, the subjects verbally rated their pain experience. The stimulus temperatures and pain ratings were then modeled with a linear function (extreme pain ratings of 0 and 100 were ignored), and the stimulation temperature that provided a pain experience of 65 was calculated.

Subjects were then moved to the scanner room and positioned supine on the scanner bed. The thermode was reattached to the lateral aspect of the ventral proximal right forearm and remained in position for the entire scanning session. For each functional imaging run, ten warm (43.0°C) and ten painful (temperature producing a moderate pain experience of 65) thermal stimuli were delivered (baseline temperature = 30.0°C, destination rate = 5.0°C/s, duration = 7.5 s, return rate 5.0°C/s) in a randomized order with a varying interstimulus interval (range = 2.5–10.0 s) over a period of 400 s, and each subject completed six runs. No feedback was provided to the subjects for the thermal stimuli, and throughout the imaging session, the subjects were instructed to remain still and not produce any movements. As a safeguard, subjects were able to stop the thermal stimulator at any time during the study if the thermal stimulation became intolerable. Following each run, the study personnel assessed the comfort level of the subjects.

2.4 Image processing

2.4.1 Motion correction—The Oxford Center for fMRI of the Brain’s (FMRIB) Software Library (FSL) and the Spinal Cord Toolbox were used for image preprocessing and statistical analyses (Cohen-Adad et al., 2014; Jenkinson et al., 2012; Smith et al., 2004). Motion correction was performed using FMRIB’s Linear Image Registration Tool with spline interpolation and a normalized correlation cost function (Jenkinson et al., 2002). To exclude areas of non-rigid motion outside of the vertebral column, a manually drawn binary mask of the vertebral column was used to weight the reference image. For the first phase of motion correction, the images across the runs were realigned to the first image of the first

run with three-dimensional rigid body realignment. To correct for slice independent motion due to the non-rigid motion of the cervical spine and physiological motion from swallowing and the respiratory cycle, a second phase of motion correction was performed in which a two-dimensional rigid realignment was performed independently for each axial slice using the mean image from the first phase of motion correction as the reference image (Cohen-Adad et al., 2009; Weber II et al., 2014). The average temporal signal to noise ratio (TSNR) across the SC was calculated for each phase of motion correction and compared using two-tailed paired t-tests. Finally, FSL's motion outlier detection tool was used to identify suspect outlier volumes using DVARS (root mean square variance of the temporal derivative of the time courses) as the metric and the default threshold (box-plot cutoff = 75th percentile + 1.5 \times interquartile range (IQR)) (Power et al., 2012).

2.4.2 Physiological noise modeling—In SC fMRI, the cardiac and respiratory cycles are significant sources of noise and can confound signal detection (Brooks et al., 2008; Kong et al., 2012). Therefore, respiratory signals, cardiac signals, and MRI triggers were collected during scanning (sampling rate = 400 Hz, PowerLab 8/30, ADInstruments Inc., Colorado Springs, CO, USA), and slice specific noise regressors were generated using FSL's physiological noise modeling (PNM) tool, which uses a model-based approach similar to the retrospective correction of physiological motion effects (RETROICOR) as described by Glover et al. (Brooks et al., 2008; Glover et al., 2000). In brief, a cardiac phase and respiratory phase were assigned to each slice, and the cardiac and respiratory signals were then modeled using a Fourier series (sine and cosine terms) with the principal frequency and the next three harmonics (16 regressors). Multiplicative terms were included to account for the interaction of the cardiac and respiratory cycles (16 additional regressors). A cerebrospinal fluid (CSF) regressor was also generated from the raw CSF signal surrounding the SC using a manually drawn CSF mask from the mean functional image generated across the six runs. In total, the physiological noise was modeled with 33 regressors, which has been recommended for SC fMRI (Kong et al., 2012).

2.4.3 Spatial normalization—For spatial normalization, the T₂-weighted structural image of the cervical spine was first cropped to include the C2 to T1 vertebrae. The C2 and T1 vertebrae were manually identified, and a vertebral landmark mask was generated. The structural image was then straightened along the SC using a binary mask of the SC, and then non-rigid registration to the MNI-Poly-AMU T₂-weighted SC template (resolution = 0.5 \times 0.5 \times 0.5 mm³) was performed using the vertebral landmarks mask (structural to template registration) (Fonov et al., 2014). The functional images were then registered to the structural image using a non-rigid deformation that was constrained to the axial plane (functional to structural registration). The deformation fields were then concatenated allowing for the forward transformation of the functional images to template space and the inverse transformation of region of interest masks in template space to native space. The transformed images at each step were visually inspected for quality control. The MNI-Poly-AMU SC template was generated from the average of the images from 16 healthy volunteers and covers the C1 to the T6 vertebral levels with the origin at the right dorsal inferior corner (Fonov et al., 2014). All reported coordinates are in the MNI-Poly-AMU SC template space. The Spinal Cord Toolbox also contains maps for the vertebral levels and probability maps

for the SC segments, which were used to summarize the location of the activity (Cadotte et al., 2015).

2.4.4 Subject and group level analyses—Slice-timing correction was performed and followed by spatial smoothing along the centerline of the SC. For spatial smoothing, the images were first straightened along the SC using a manually drawn SC mask, a $2 \times 2 \times 6$ mm³ full width half maximum (FWHM) Gaussian smoothing kernel was applied, and the images were then de-straightened as original. High pass temporal filtering was then performed (sigma = 90 s), and statistical maps of the preprocessed times series for each run were generated using FMRIB's Improved Linear Model (FILM) with prewhitening (Woolrich et al., 2001; Worsley, 2001). The design matrix included the standard hemodynamic response function (gamma, phase 0 s, standard deviation 3 s, average lag 6 s) convolved thermal stimulation vectors (from the thermode temperature output) for the warm and painful stimuli as explanatory variables; and the temporal derivatives of the task vectors, the physiological noise vectors, the six motion parameters from the first phase of motion correction, the derivatives of the motion parameters, and the temporal masks of any outlier volumes were included as covariates of no interest. Four contrasts were defined: two for the warm and painful stimuli relative to baseline (warm and painful stimuli) and two for the difference between the warm and painful stimuli (warm > painful and painful > warm contrasts). Average subject level activation maps were then calculated across the six runs for each contrast using a fixed-effects model. Voxels with a $p < 0.05$ (uncorrected) were considered active at the subject level. No correction for multiple comparisons was performed at the subject level due to the restricted volume of interrogation as the SC contains a much smaller number of voxels. Furthermore, the presence of false positives was explored through a control analysis (see Control analysis).

For the group analysis, spatial normalization of the statistical images from the subject level analyses to the SC template was performed, and average group activation maps for each contrast were generated using FMRIB's Local Analysis of Mixed Effects (FLAME) stages 1 and 2 (Beckmann et al., 2003; Woolrich, 2008; Woolrich et al., 2004). Significant activations at the group level were identified by using a cluster-level, family-wise error (FWE) corrected threshold of $p < 0.05$ (cluster defining threshold $p < 0.05$, cluster size = 2179 voxels in template space, volume = 272.4 mm³) to correct for multiple comparisons (Worsley, 2001).

2.5 Additional analyses

In addition to the detection of group and subject level activity, the following analyses were performed to characterize the results:

2.5.1 Spatial analysis—The number of active voxels in the left, right, dorsal, and ventral hemicords and at the C3, C4, C5, C6, and C7 vertebral levels was calculated for each contrast. Left-right (LR) and dorsal-ventral (DV) indices were calculated at the subject level (Seghier, 2008). The indices were calculated by dividing the difference in the number of active voxels between the respective hemicords by the sum (number of active voxels in the entire SC). For the LR index, a value of +1.0 indicates that all active voxels were located in the left hemicord while a value of -1.0 indicates that all active voxels were located in the

right hemicord. For the DV index, a value of +1.0 indicates that all active voxels were located in the dorsal hemicord while a value of -1.0 indicates that all active voxels were located in the ventral hemicord. A Wilcoxon signed-rank test with a hypothesized median of 0 was performed to test for significant localization of the active voxels.

2.5.2 Control analysis—As an additional control for false positives, the thermal stimulation results were compared to a control analysis in which the temperature vectors were shuffled across the subjects and the runs, and each run was then reanalyzed using the shuffled thermal stimulation vectors. Group average activation maps were generated for the control analysis, and the number of active voxels and the average Z-score of the active voxels were calculated and compared to thermal stimulation. For each subject, the number of active voxels in the control condition and the average Z-score of the active voxels were also calculated and compared to thermal stimulation using two-tailed paired t-tests.

2.5.3 Signal change—FSL's results interrogation tool (FEATQuery) was used to calculate the average percent signal change of the active voxels. The number of active voxels and the average percent signal change of the active voxels was compared between the warm and painful stimuli using the subject level activation maps from the average of the six runs and two-tailed paired t-tests. To investigate how the signal changed over the runs, a repeated measures analysis of variance (ANOVA) with a linear contrast was performed to assess for a linear increase or decrease in the number of active voxels and the average percent signal change of the active voxels across the six runs for both the warm and painful stimuli.

2.5.4 Reliability analysis—To assess the reliability of the activity across the runs, average group activation maps from each run were generated for the warm and painful stimuli, and the spatial localization of the activity was assessed. For each run, the number of active voxels and the average Z-score of the active voxels were calculated, and Spearman's correlations were performed to identify an increase or decrease in the number of active voxels and the average Z-score of the active voxels across the runs. To assess within subject variability in the spatial localization of the activity across the runs, the center-of-gravity (COG) of the active voxels along the x-, y-, and z-axes (in template space) was calculated for each run and compared to the COG of the active voxels from the average of the six runs for each subject. Finally, intraclass correlation coefficients (ICC(3,1)) were also calculated using the ICC Toolbox in SPM5 with MATLAB (Version R2013b, The Mathworks, Inc., Natick, MA, USA) to assess the agreement of the subject activations from run to run (Caceres et al., 2009). For the reliability analyses, the group average activation maps were thresholded at a $p < 0.05$ (uncorrected).

2.5.5 Power analysis—To investigate the effect of the number of runs on the activity, average group activation maps were generated with the addition of subsequent runs (Run 1, Runs 1–2, Runs 1–3, Runs 1–4, Runs 1–5, and Runs 1–6). For each analysis, the number of active voxels and the average Z-score of the active voxels were calculated, and a Spearman's correlations were performed to identify a monotonic relationship between the number of runs and the number of active voxels and the average Z-score of the active voxels. For the

power analysis, the group average activation maps were thresholded at a $p < 0.05$ (uncorrected).

2.5.6 Multi-voxel pattern analysis—A within subject run-wise multi-voxel pattern analysis (MVPA) using a linear support vector machine classifier and leave-one-run-out cross-validation was performed to decode the warm and painful stimuli based on the corresponding activity patterns (Chang and Lin, 2011). The MVPA was performed across the entire SC and within the left, right, dorsal, and ventral hemicords. The average accuracy across the subjects was compared to chance (50% accuracy) using one-sample two-tailed t-tests with Bonferroni correction for multiple comparisons.

2.5.7 Statistical testing—For all non-imaging statistical tests, IBM SPSS Statistics for Windows Version 22.0 (IBM Corp., Armonk, NY) was used, and an $\alpha < 0.05$ was used as the threshold for statistical significance.

3. Results

All subjects successfully completed each run of data collection. Motion correction improved the quality of the data as indicated by the increase in the average TSNR over the SC. The average TSNR \pm one standard error (SE) significantly increased from 10.5 ± 0.6 arbitrary units (au) to 14.7 ± 0.2 au with the first phase of motion correction ($t = 10.405$, $p < 0.001$) and significantly increased from the first phase of motion correction to 15.5 ± 0.2 au with the second phase of motion correction ($t = 8.071$, $p < 0.001$). Following all preprocessing steps (motion correction, slice-timing correction, spatial smoothing, and temporal filtering), the average TSNR was 74.4 ± 3.2 au. The average percentage of the volumes identified as motion outlier volumes \pm one SE was $1.5 \pm 0.3\%$. Spatial normalization from native space to template space was successfully performed for each subject. The average pain threshold \pm one SE was $45.2 \pm 0.5^\circ\text{C}$ (range = $42.1\text{--}48.3^\circ\text{C}$), and the average painful stimulus temperature was $46.6 \pm 0.4^\circ\text{C}$ (range = $44.3\text{--}49.1^\circ\text{C}$). One subject reported a mild pain experience (NRS < 35) at the warm stimulus temperature of 43.0°C (Hawker et al., 2011).

3.1 Group level activity

We hypothesized that the activity during thermal stimulation would be localized primarily to the ipsilateral dorsal quadrant and proportional to the stimulus temperature at the group and subject level. At the group level, activity was detected for the warm and painful stimuli and for the painful $>$ warm contrasts while no activity was detected for the warm $>$ painful contrast, demonstrating that the signal change was greater for the painful stimulus, as expected (Table 1). However, the activity was not lateralized to the ipsilateral hemicord for either the warm or painful stimuli. For the painful stimulus, the activity was more evenly distributed across the right and left hemicords while the activity for the warm stimulus was more localized to the left hemicord. Although lateralization of the activity was not present, both the warm and painful stimuli resulted in more active voxels in the dorsal hemicord. In comparison, the painful $>$ warm contrast resulted in the opposite localization of the activity with more active voxels in the ventral hemicord. Thermal stimulation of the lateral aspect of the ventral proximal right forearm was expected to result in activity primarily localized to

the C6 SC segment. Instead, the activity detected was more distributed along the superior-inferior axis with the activity expanding across the C3–C7 vertebral bodies corresponding to the C4 to C8 SC segments (Figure 2 and 3A–C). The removal of outliers using FSL's automatic outlier de-weighting or the exclusion of the subject that experienced a mild pain experience with the warm stimulus had no appreciable effect on the group activity. Group average activation maps without correction for multiple comparisons (uncorrected $p < 0.05$) for the warm and painful stimuli have been provided for reference (Supplementary Figure 1).

3.2 Subject level activity

As with the group level activity, the activity at the subject level was expected to be localized to the ipsilateral dorsal quadrant. Similar to the group level activity, no significant localization of the activity to the left or right hemicords was present for the warm (2/12 subjects with LR index > 0 , median LR index = -0.15 , IQR = 0.36 , $z = -1.883$, $p = 0.060$) or painful (5/12 subjects with LR index > 0 , median LR index = -0.08 , IQR = 0.47 , $z = -0.706$, $p = 0.480$) stimuli (Figure 4A). Despite the absence of lateralization of the activity, the activity was significantly localized to the dorsal hemicord for both the warm (12/12 subjects with DV index > 0 , median DV index = 0.41 , IQR = 0.34 , $z = 3.059$, $p = 0.002$) and painful (9/12 subjects with DV index > 0 , median DV index = 0.24 , IQR = 0.39 , $z = 1.961$, $p < 0.050$) stimuli (Figure 4B). In contrast, no significant localization of the activity to the left or right hemicords (7/12 subjects with LR index > 0 , median LR index = 0.04 , IQR = 0.24 , $z = 0.000$, $p = 1.000$) or the dorsal or ventral hemicords (4/12 subjects with DV index > 0 , median DV index = -0.05 , IQR = 0.24 , $z = -0.471$, $p = 0.638$) was present for the painful $>$ warm contrast (Figure 3D).

3.3 Control analysis

As an additional control for false positive activations, the thermal stimulation results were compared to a control analysis. As expected, the control analysis resulted in no group activity for either the warm or painful stimuli. Similar findings were also present at the subject level (Figure 5). The average number of active voxels \pm one SE for thermal stimulation was 212.6 ± 50.7 for the warm stimulus, which tended to be greater than the control (114.7 ± 18.4 , $t = 1.986$, $p = 0.073$). After removal of an outlier observation, the number of active voxels for the warm stimulus significantly exceeded that of the control (Supplementary Figure 2). The average Z-score of the active voxels \pm one SE for thermal stimulation was 2.32 ± 0.07 for the warm stimulus, which was significantly greater than the control (2.03 ± 0.03 , $t = 3.715$, $p = 0.003$). For the painful stimulus, the number of active voxels for thermal stimulation was 371.4 ± 70.3 , which was significantly greater than the control (124.5 ± 18.3 , $t = 3.440$, $p = 0.006$), and the average Z-score of the active voxels for thermal stimulation was 2.32 ± 0.07 , which was significantly greater than the control (2.09 ± 0.03 , $t = 2.677$, $p = 0.022$). Overall, the spatial extent and magnitude of the activity during thermal stimulation exceeded that of the control analysis at both the group and subject level.

3.4 Signal change

We expected the spatial extent and magnitude of the activity to be greater for the painful stimulus than the warm stimulus at the subject level. Across the subjects, the average

number of active voxels was 371.4 ± 70.3 for the painful stimulus, which was significantly greater than the warm stimulus (212.6 ± 50.7 , $t = 2.242$, $p = 0.047$) (Figure 6A). The average percent signal change \pm one SE was also significantly greater for the painful stimulus ($0.38 \pm 0.01\%$) compared to the warm stimulus ($0.33 \pm 0.02\%$, $t = 2.385$, $p = 0.036$) (Figure 6B). Additionally, we examined the change in the activity across the six runs at the subject level (Figure 7). No significant linear increase or decrease in the number of active voxels was present for the warm stimulus (F-score = 2.461, $p = 0.145$). The number of active voxels tended to increase across the six runs for the painful stimulus, but this trend was not significant (F-score = 3.831, $p = 0.076$). No linear increase or decrease in the average percent signal change of the active voxels across the runs was present for either the warm (F-score = 0.050, $p = 0.827$) or painful (F-score = 0.488, $p = 0.499$) stimuli.

3.5 Multi-voxel pattern analysis

To assess the amount of pain-related information present in the SC, we utilized a MVPA to decode the thermal stimuli based on the distributed patterns of SC activity. MVPA was successfully able to decode the warm and painful stimuli better than chance across the entire SC (average percent accuracy \pm one SE = $66.7 \pm 2.9\%$, $t = 5.745$, $p < 0.001$). The MVPA was also able to successfully decode the warm and painful stimuli better than chance in the left (average percent accuracy = $61.8 \pm 2.2\%$, $t = 5.451$, $\alpha/2 = 0.025$, $p < 0.001$) and right (average percent accuracy = $66.0 \pm 4.3\%$, $t = 3.727$, $\alpha/2 = 0.025$, $p = 0.003$) hemispheres and the dorsal (average percent accuracy = $65.3 \pm 3.4\%$, $t = 4.525$, $\alpha/2 = 0.025$, $p < 0.001$) and ventral (average percent accuracy = $66.7 \pm 3.4\%$, $t = 4.899$, $\alpha/2 = 0.025$, $p < 0.001$) hemispheres (Figure 8C).

3.6 Reliability analysis

Despite several studies using fMRI to detect SC activity during noxious thermal stimulation, the reliability of SC fMRI for assessing nociceptive processing needs to be further established (Kolesar et al., 2015), and therefore, assessing the reliability of the activity across consecutive runs was a major aim of this study. At the group and subject level, activity was present for each run for both the warm and painful stimuli. However, no consistent localization of the activity across the runs was present at the group level (Supplementary Figure 3). Similarly, at the subject level, no consistent localization was present, but the activity was located more dorsally for each of the six runs (Supplementary Table 1). At the group level, no significant linear increase or decrease in the total number of active voxels ($\rho = 0.429$, $p = 0.397$) or the average Z-score of the active voxels ($\rho = 0.257$, $p = 0.623$) was present across the runs for the warm stimulus (Supplementary Figure 3C–D). In contrast, a significant increase in the total number of active voxels ($\rho = 0.886$, $p = 0.019$) was present across the runs at the group level for the painful stimulus, but no significant change in the average Z-score of the active voxels ($r = 0.543$, $p = 0.266$) was present (Supplementary Figure 3E–F). Across subjects and runs, considerable variability was present with the COGs of the activation maps along the x-, y-, and z-axes (Supplementary Figure 4). The considerable spatial variability across the runs was characterized by low median ICCs \pm one SE across the runs for the warm and painful stimuli, which were 0.067 ± 0.002 and 0.090 ± 0.001 , respectively. Averaging across the first (runs 1–3) and second (runs 4–6) halves of the data reduced the variability and increased the

median ICC to 0.193 ± 0.004 and 0.258 ± 0.003 for the warm and painful stimuli, respectively.

3.7 Power analysis

Finally, to aid in the design of future studies, the effect that the number of runs had on the activity was assessed. Group and subject level activity was present for each analysis (Run 1, Runs 1–2, Runs 1–3, Runs 1–4, Runs 1–5, and Runs 1–6) (Supplementary Figure 5 A–B). The total number of active voxels significantly increased with the addition of subsequent runs for both the warm ($\rho = 1.000$, $p < 0.001$) and painful (Spearman's $\rho = 1.000$, $p < 0.001$) stimuli (Supplementary Figure 5C and E). However, the addition of subsequent runs had no significant effect on the average Z-score of the active voxels for either the warm ($\rho = 0.486$, $p = 0.329$) or painful ($\rho = 0.314$, $p = 0.544$) stimuli (Supplementary Figure 5D and F).

4. Discussion

Cervical SC activity was detected using fMRI during thermal stimulation with warm and painful stimuli. At the group and subject level, the spatial extent and magnitude of the activity exceeded that of the control analysis, the activity was localized more to the dorsal hemicord, and the spatial extent and magnitude of the activity was greater for the painful stimulus than the warm stimulus. Furthermore, we were able to use MVPA to decode the stimuli based on their activity patterns. Taken together, we were able to successfully detect and characterize cervical SC activity during thermal stimulation with fMRI.

In the present study, thermal stimuli were applied to the lateral aspect of the ventral proximal right forearm. Cutaneous thermal and thermal-pain sensations are mediated primarily by A δ - and C-fiber thermoreceptors and temperature-sensitive nociceptors, which project mainly to neurons in the ipsilateral dorsal horn of the SC (Green, 2004; Willis and Westlund, 1997). As the first site of sensory processing, we hypothesized that the activity would be localized to the right dorsal quadrant of the SC. The activity was localized more dorsally at the group and subject level; however, the activity was not localized to the right hemicord. At the subject level, no significant localization of the activity to the left or right hemicord was present, and at the group level, the activity for the painful stimulus was more evenly distributed across the right and left hemicords while the activity for the warm stimulus was localized more to the left hemicord. The absence of lateralization of the activity to the ipsilateral hemicord has been reported in previous SC fMRI studies using noxious thermal stimulation in humans (Geuter and Buchel, 2013; Summers et al., 2010) and non-human primates (Yang et al., 2015) and likely reflects the underlying complexity of SC sensory processing. The interneuronal networks within the dorsal horn not only relay sensory information to higher centers (i.e., brainstem and thalamus) but also actively integrate and modulate the sensory signals within the SC (Willis and Westlund, 1997). This large network of intrinsic neurons has been shown to influence both sensory and motor processing not only within the same hemicord but also between hemicords (Chung and Coggeshall, 1983; Nathan and Smith, 1959; Petko and Antal, 2000; Petko et al., 2004; Pierrot-Deseilligny and Marchand-Pauvert, 2002; Soteropoulos et al., 2013). These networks also receive excitatory

and inhibitory inputs from higher centers, which further modulate SC processing (Heinricher et al., 2009; Yang and Gorassini, 2006). Recently, intrinsic resting state networks between the left and right dorsal horns and the left and right ventral horns were identified with fMRI in humans (Barry et al., 2016; Barry et al., 2014) and non-human primates (Kong et al., 2014), and injury to the SC has been demonstrated to disrupt these networks (Chen et al., 2015). Based on these findings, the coordinated activity between the hemicords may represent the state of normal sensory processing, explaining the absence of the lateralization of the activity detected in this study. In contrast, we previously demonstrated robust lateralization of SC activity with fMRI during a left- or right-sided upper extremity motor task (Weber et al., 2016). The lateralization in the previous study was most consistent when contrasting the left- and right-sided activity rather than modeling them individually to baseline. A similar experiment contrasting left- and right-sided thermal stimulation may have demonstrated lateralization of the activity; in the present study, however, we chose to manipulate the intensity of the stimulus not the location.

Although the activity was localized more dorsally, the activity extended into the ventral hemicord. In primates, the spinothalamic tract is the major pathway relaying thermal and nociceptive input from the SC to the thalamus (Willis and Westlund, 1997). While most spinothalamic neurons originate in the dorsal horn, sensory processing is not exclusively localized to the dorsal horn. Autoradiographic studies have demonstrated metabolic activity extending into the ipsilateral and contralateral ventral horns during innocuous and noxious thermal stimulation in rats (Coghill et al., 1993; Coghill et al., 1991), and in primates, between 8–17% of spinothalamic neurons originate in the intermediate zone and ventral horn (Apkarian and Hodge, 1989). Based on this, some ventral activity would be expected. The ventral activity may in part also be due to reflexive motor activity (Floeter et al., 1998). If this were the case, greater reflexive motor activity (ventral hemicord) would be expected from the painful stimulus (Chan and Dallaire, 1989). When modeling the difference between the stimuli (painful > warm), we found that the activity was no longer localized to the dorsal hemicord at the subject level, and the group activity was more localized to the ventral hemicord, which suggests that some of the ventral activity may be reflexive motor activity. As subjects were asked to remain still during scanning, the ventral activity could also reflect descending inhibition of reflexive motor activity. Electromyography could potentially be used to characterize any stimulus-related motor activity in future studies.

The stimulation site classically corresponds to the C6 dermatome, and therefore, we hypothesized that the activity should be located primarily within the C6 SC segment (Moore et al., 2014). However, a broader superior-inferior distribution of the activity extending across the C4–C8 SC segments was observed instead. The broader superior-inferior distribution may reflect the variability in the location of dermatomes across the subjects. The classic dermatome maps are largely inaccurate, show no overlap of innervation from adjacent SC segments, and fail to provide information on intersubject variability (Lee et al., 2008). Therefore, consistent stimulation of only the C6 dermatome across the subjects was not likely. Additionally, the broader superior-inferior distribution of the activity may also be explained by the ascending and descending collaterals of Lissauer's tract in which primary afferent fibers may ascend or descend several SC segments before even entering the SC gray matter (Coggeshall et al., 1981; Light and Perl, 1979; Sugiura et al., 1986). With this

understanding, even specific stimulation of the C6 dermatome would likely result in activity spanning several SC segments. Finally, the activity detected was not likely specifically sensory as the thermal stimuli probably resulted in some reflexive motor activity. Any reflexive motor activity in the upper arm, shoulder, or neck muscles could have also contributed to the activity in more superior SC segments (Moore et al., 2014).

Repeated noxious thermal stimuli can result in sensitization within the nociceptive pathways leading to a leftward shift in the temperature-pain response function causing painful stimuli to become more painful (i.e., hyperalgesia) and previously non-painful stimuli to become painful (i.e., allodynia) (Latremoliere and Woolf, 2009; Woolf, 1983). While pain ratings were not obtained during scanning, the subjects anecdotally reported an increase in their pain experience across the six runs, and temporary mild erythema was typically present over the stimulation site at the end of the study. Considering these findings and the stimulation protocol used in this study, some sensitization to the thermal stimuli across the runs likely occurred (Jurgens et al., 2014). To assess whether indicators of sensitization were present in the data, we looked for an increase in the number of active voxels and the average percent signal change of the active voxels across the runs. From this, we identified a significant increase in the number of active voxels across the runs for the painful stimuli at the group level, which may reflect sensitization. Based on the stimulation protocol, both peripheral and central sensitization may have occurred (Jurgens et al., 2014). The increase in the spatial extent of the activity may be due to decreased thresholds of peripheral receptors and their central targets, the unmasking of silent receptors, and/or greater reflexive motor activity (Chan and Dallaire, 1989; Latremoliere and Woolf, 2009). Sensitization would be expected to also lead to an increase in signal change; however, no increase in signal intensity across the runs was identified in this study. Similar findings have been previously reported using a temporal summation of second pain model (Bosma et al., 2015). However, additional studies with a larger sample size are needed to thoroughly investigate the fMRI correlates of spinal sensitization induced by noxious painful stimuli.

A major aim of this study was to investigate the reliability of the activity with thermal stimulation from run to run. Overall, the location of the activity across the runs was quite variable at the group and subject level (intrasubject and intersubject), which is reflected in the low ICCs across the runs. Despite this, the activity tended to be more dorsally localized (i.e., the DV index was positive for each of the runs and the COGs tended to be distributed dorsally). Greater consistency of the location of the activity was expected, and overall, the underlying reason for the variability is unknown. Sensitization to the repeated thermal stimuli may have contributed to some of the variability as the signal was likely not constant across the runs. Averaging across more than one run seems to reduce the spatial variability and is recommended for future studies.

Despite the substantial spatial variability across the runs, MVPA was able to successfully decode the warm and painful stimuli based on their activity patterns. Previous studies have applied machine-learning algorithms to distinguish between warm and painful stimuli in the brain (Brown et al., 2011; Wager et al., 2013). This is the first report in the SC. While the overall accuracy of the decoding model was low, the results demonstrated that sufficient

information was present in the pattern of the SC activity to successfully decode the experimental conditions.

A major limitation in this study was the absence of subject reported pain ratings throughout scanning. Pain ratings could have confirmed that sensitization occurred and may have provided additional insights into the nature of the activity. A second limitation is that the spatial normalization algorithm for the transformation from native to template space uses the vertebral levels and not the SC segments to register along the superior-inferior axis. Recent work suggests that the location of the SC segments in relation to the vertebral bodies varies appreciably across subjects (Cadotte et al., 2015). The effects that this variation has on the present results are unknown, but it prevents exact correspondence of the SC anatomy between subjects. Accounting for this variation with more advanced normalization algorithms should allow for even more robust and accurate group analyses (Cadotte et al., 2014). Finally, the greater localization of the warm stimulus activity to the left hemicord at the group level using the *a priori* level of statistical significance was not expected and may indicate that the study was underpowered to adequately detect the signal change from the warm stimulus. The reported TSNR and signal change can be used to adequately power future studies to sufficiently characterize the spatial extent of the activity resulting from lower intensity stimuli.

5. Conclusion

In conclusion, we were able to successfully detect cervical SC activity during warm and painful thermal stimulation with fMRI. Both stimuli resulted in activity at the group and subject level, and the activity was localized more to the dorsal hemicord. The spatial localization of the activity varied considerably from run to run, but despite this variability, a machine-learning algorithm was able to successfully decode the stimuli in the spinal cord based on the distributed pattern of the activity.

Supplementary Material

Refer to Web version on PubMed Central for supplementary material.

Acknowledgments

Research reported in this publication was supported by the National Center for Complementary and Integrative Health under award number F32AT007800 and the National Institute of Child Health and Development under award number T32HD057845. The content is solely the responsibility of the authors and does not necessarily represent the official views of the National Institutes of Health.

Abbreviations

SC	spinal cord
BOLD	blood oxygen level dependent
MR	magnetic resonance
MRI	magnetic resonance imaging

fMRI	functional magnetic resonance imaging
SPACE	sampling perfection with application optimized contrast using different flip angle evolutions
FMRIB	Oxford Center for Functional MRI of the Brain
FSL	FMRIB's Software Library

References

- Apkarian AV, Bushnell MC, Treede RD, Zubieta JK. Human brain mechanisms of pain perception and regulation in health and disease. *Eur J Pain*. 2005; 9:463–484. [PubMed: 15979027]
- Apkarian AV, Hodge CJ. Primate spinothalamic pathways: I. A quantitative study of the cells of origin of the spinothalamic pathway. *J Comp Neurol*. 1989; 288:447–473. [PubMed: 2477420]
- Barry RL, Rogers BP, Conrad BN, Smith SA, Gore JC. Reproducibility of resting state spinal cord networks in healthy volunteers at 7 Tesla. *Neuroimage*. 2016; 133:31–40. [PubMed: 26924285]
- Barry RL, Smith SA, Dula AN, Gore JC. Resting state functional connectivity in the human spinal cord. *Elife*. 2014; 3:e02812. [PubMed: 25097248]
- Beckmann CF, Jenkinson M, Smith SM. General multilevel linear modeling for group analysis in fMRI. *Neuroimage*. 2003; 20:1052–1063. [PubMed: 14568475]
- Bosma RL, Ameli Mojarad E, Leung L, Pukall C, Staud R, Stroman PW. Neural correlates of temporal summation of second pain in the human brainstem and spinal cord. *Hum Brain Mapp*. 2015
- Brooks JC, Beckmann CF, Miller KL, Wise RG, Porro CA, Tracey I, Jenkinson M. Physiological noise modelling for spinal functional magnetic resonance imaging studies. *Neuroimage*. 2008; 39:680–692. [PubMed: 17950627]
- Brooks JC, Kong Y, Lee MC, Warnaby CE, Wanigasekera V, Jenkinson M, Tracey I. Stimulus site and modality dependence of functional activity within the human spinal cord. *J Neurosci*. 2012; 32:6231–6239. [PubMed: 22553029]
- Brown JE, Chatterjee N, Younger J, Mackey S. Towards a physiology-based measure of pain: patterns of human brain activity distinguish painful from non-painful thermal stimulation. *PLoS One*. 2011; 6:e24124. [PubMed: 21931652]
- Caceres A, Hall DL, Zelaya FO, Williams SC, Mehta MA. Measuring fMRI reliability with the intra-class correlation coefficient. *Neuroimage*. 2009; 45:758–768. [PubMed: 19166942]
- Cadotte DW, Bosma R, Mikulis D, Nugaeva N, Smith K, Pokrupa R, Islam O, Stroman PW, Fehlings MG. Plasticity of the injured human spinal cord: insights revealed by spinal cord functional MRI. *PLoS One*. 2012; 7:e45560. [PubMed: 23029097]
- Cadotte, DW.; Cadotte, A.; Cohen-Adad, J.; Fleet, D.; Livne, M.; Mikulis, D.; Fehlings, MG. Resolving the anatomic variability of the human cervical spinal cord: a solution to facilitate advanced neural imaging. Proceedings of the 22th Annual Meeting of the International Society for Magnetic Resonance in Medicine; Milan, Italy. 2014.
- Cadotte DW, Cadotte A, Cohen-Adad J, Fleet D, Livne M, Wilson JR, Mikulis D, Nugaeva N, Fehlings MG. Characterizing the location of spinal and vertebral levels in the human cervical spinal cord. *AJNR Am J Neuroradiol*. 2015; 36:803–810. [PubMed: 25523587]
- Cahill CM, Stroman PW. Mapping of neural activity produced by thermal pain in the healthy human spinal cord and brain stem: a functional magnetic resonance imaging study. *Magn Reson Imaging*. 2011; 29:342–352. [PubMed: 21247717]
- Carstens E, Yokota T, Zimmermann M. Inhibition of spinal neuronal responses to noxious skin heating by stimulation of mesencephalic periaqueductal gray in the cat. *J Neurophysiol*. 1979; 42:558–568. [PubMed: 422977]
- Chan CW, Dallaire M. Subjective pain sensation is linearly correlated with the flexion reflex in man. *Brain Res*. 1989; 479:145–150. [PubMed: 2924143]
- Chang CC, Lin CJ. LIBSVM: A library for support vector machines. *ACM Trans Intell Syst Technol*. 2011; 2:1–27.

- Chen LM, Mishra A, Yang PF, Wang F, Gore JC. Injury alters intrinsic functional connectivity within the primate spinal cord. *Proc Natl Acad Sci U S A*. 2015; 112:5991–5996. [PubMed: 25902510]
- Chung K, Coggeshall RE. Propriospinal fibers in the rat. *J Comp Neurol*. 1983; 217:47–53. [PubMed: 6875052]
- Coggeshall RE, Chung K, Chung JM, Langford LA. Primary afferent axons in the tract of Lissauer in the monkey. *J Comp Neurol*. 1981; 196:431–442. [PubMed: 7217365]
- Coghill RC, Mayer DJ, Price DD. The roles of spatial recruitment and discharge frequency in spinal cord coding of pain: a combined electrophysiological and imaging investigation. *Pain*. 1993; 53:295–309. [PubMed: 8351159]
- Coghill RC, Price DD, Hayes RL, Mayer DJ. Spatial distribution of nociceptive processing in the rat spinal cord. *J Neurophysiol*. 1991; 65:133–140. [PubMed: 1999727]
- Cohen-Adad, J.; De Leener, B.; Benhamou, M.; Lévy, S.; Touati, J.; Cadotte, D.; Fleet, D.; Cadotte, A.; Fehlings, M.; Pelletier Paquette, JP.; Thong, W.; Taso, M.; Collins, L.; Callot, V.; Fonov, V. Spinal Cord Toolbox: an open-source framework for processing spinal cord MRI data. 20th Annual Meeting of the Organization for Human Brain Mapping; Hamburg, Germany. 2014.
- Cohen-Adad, J.; Rossignol, S.; Hoge, RD. Slice-by-slice motion correction in spinal cord fMRI: SliceCorr. Proceedings of the 17th Annual Meeting of the International Society for Magnetic Resonance in Medicine; Honolulu, USA. 2009.
- Dobek CE, Beynon ME, Bosma RL, Stroman PW. Music modulation of pain perception and pain-related activity in the brain, brain stem, and spinal cord: a functional magnetic resonance imaging study. *J Pain*. 2014; 15:1057–1068. [PubMed: 25077425]
- Eippert F, Finsterbusch J, Bingel U, Buchel C. Direct evidence for spinal cord involvement in placebo analgesia. *Science*. 2009; 326:404. [PubMed: 19833962]
- Endo T, Spenger C, Westman E, Tominaga T, Olson L. Reorganization of sensory processing below the level of spinal cord injury as revealed by fMRI. *Exp Neurol*. 2008; 209:155–160. [PubMed: 17988666]
- Floeter MK, Gerloff C, Kouri J, Hallett M. Cutaneous withdrawal reflexes of the upper extremity. *Muscle Nerve*. 1998; 21:591–598. [PubMed: 9572238]
- Fonov VS, Le Troter A, Taso M, De Leener B, Leveque G, Benhamou M, Sdika M, Benali H, Pradat PF, Collins DL, Callot V, Cohen-Adad J. Framework for integrated MRI average of the spinal cord white and gray matter: the MNI-Poly-AMU template. *Neuroimage*. 2014; 102(Pt 2):817–827. [PubMed: 25204864]
- Geuter S, Buchel C. Facilitation of pain in the human spinal cord by nocebo treatment. *J Neurosci*. 2013; 33:13784–13790. [PubMed: 23966699]
- Glover GH, Li TQ, Ress D. Image-based method for retrospective correction of physiological motion effects in fMRI: RETROICOR. *Magn Reson Med*. 2000; 44:162–167. [PubMed: 10893535]
- Green BG. Temperature perception and nociception. *J Neurobiol*. 2004; 61:13–29. [PubMed: 15362150]
- Hackam DG, Redelmeier DA. Translation of research evidence from animals to humans. *JAMA*. 2006; 296:1731–1732. [PubMed: 17032985]
- Hawker GA, Mian S, Kendzerska T, French M. Measures of adult pain: Visual Analog Scale for Pain (VAS Pain), Numeric Rating Scale for Pain (NRS Pain), McGill Pain Questionnaire (MPQ), Short-Form McGill Pain Questionnaire (SF-MPQ), Chronic Pain Grade Scale (CPGS), Short Form-36 Bodily Pain Scale (SF-36 BPS), and Measure of Intermittent and Constant Osteoarthritis Pain (ICOAP). *Arthritis Care Res (Hoboken)*. 2011; 63(Suppl 11):S240–252. [PubMed: 22588748]
- Heinricher MM, Tavares I, Leith JL, Lumb BM. Descending control of nociception: Specificity, recruitment and plasticity. *Brain Res Rev*. 2009; 60:214–225. [PubMed: 19146877]
- Jenkinson M, Bannister P, Brady M, Smith S. Improved optimization for the robust and accurate linear registration and motion correction of brain images. *Neuroimage*. 2002; 17:825–841. [PubMed: 12377157]
- Jenkinson M, Beckmann CF, Behrens TE, Woolrich MW, Smith SM. FSL. *Neuroimage*. 2012; 62:782–790. [PubMed: 21979382]

- Jurgens TP, Sawatzki A, Henrich F, Magerl W, May A. An improved model of heat-induced hyperalgesia–repetitive phasic heat pain causing primary hyperalgesia to heat and secondary hyperalgesia to pinprick and light touch. *PLoS One*. 2014; 9:e99507. [PubMed: 24911787]
- Khan HS, Stroman PW. Inter-individual differences in pain processing investigated by functional magnetic resonance imaging of the brainstem and spinal cord. *Neuroscience*. 2015; 307:231–241. [PubMed: 26335379]
- Kolesar TA, Fiest KM, Smith SD, Kornelsen J. Assessing Nociception by fMRI of the Human Spinal Cord: A Systematic Review. *Magn Reson Insights*. 2015; 8:31–39. [PubMed: 26543372]
- Kong Y, Eippert F, Beckmann CF, Andersson J, Finsterbusch J, Buchel C, Tracey I, Brooks JC. Intrinsically organized resting state networks in the human spinal cord. *Proc Natl Acad Sci U S A*. 2014; 111:18067–18072. [PubMed: 25472845]
- Kong Y, Jenkinson M, Andersson J, Tracey I, Brooks JC. Assessment of physiological noise modelling methods for functional imaging of the spinal cord. *Neuroimage*. 2012; 60:1538–1549. [PubMed: 22178812]
- Latremoliere A, Woolf CJ. Central sensitization: a generator of pain hypersensitivity by central neural plasticity. *J Pain*. 2009; 10:895–926. [PubMed: 19712899]
- Lee MW, McPhee RW, Stringer MD. An evidence-based approach to human dermatomes. *Clin Anat*. 2008; 21:363–373. [PubMed: 18470936]
- Lichy MP, Wietek BM, Mugler JP 3rd, Horger W, Menzel MI, Anastasiadis A, Siegmann K, Niemeyer T, Konigsrainer A, Kiefer B, Schick F, Claussen CD, Schlemmer HP. Magnetic resonance imaging of the body trunk using a single-slab, 3-dimensional, T2-weighted turbo-spin-echo sequence with high sampling efficiency (SPACE) for high spatial resolution imaging: initial clinical experiences. *Invest Radiol*. 2005; 40:754–760. [PubMed: 16304477]
- Light AR, Perl ER. Spinal termination of functionally identified primary afferent neurons with slowly conducting myelinated fibers. *J Comp Neurol*. 1979; 186:133–150. [PubMed: 109477]
- Lilja J, Endo T, Hofstetter C, Westman E, Young J, Olson L, Spenger C. Blood oxygenation level-dependent visualization of synaptic relay stations of sensory pathways along the neuroaxis in response to graded sensory stimulation of a limb. *J Neurosci*. 2006; 26:6330–6336. [PubMed: 16763041]
- Lin Q, Peng Y, Willis WD. Glycine and GABAA antagonists reduce the inhibition of primate spinothalamic tract neurons produced by stimulation in periaqueductal gray. *Brain Res*. 1994; 654:286–302. [PubMed: 7987678]
- Maehara M, Ikeda K, Kurokawa H, Ohmura N, Ikeda S, Hirokawa Y, Maehara S, Utsunomiya K, Tanigawa N, Sawada S. Diffusion-weighted echo-planar imaging of the head and neck using 3-T MRI: Investigation into the usefulness of liquid perfluorocarbon pads and choice of optimal fat suppression method. *Magn Reson Imaging*. 2014; 32:440–445. [PubMed: 24582547]
- Malisza KL, Stroman PW. Functional imaging of the rat cervical spinal cord. *J Magn Reson Imaging*. 2002; 16:553–558. [PubMed: 12412032]
- Mansour AR, Farmer MA, Baliki MN, Apkarian AV. Chronic pain: the role of learning and brain plasticity. *Restor Neurol Neurosci*. 2014; 32:129–139. [PubMed: 23603439]
- Mao J. Translational pain research: achievements and challenges. *J Pain*. 2009; 10:1001–1011. [PubMed: 19628433]
- Moore KL, Dalley AF, Agur AMR. *Clinically oriented anatomy*. 2014
- Mugler JP 3rd, Bao S, Mulkern RV, Guttman CR, Robertson RL, Jolesz FA, Brookeman JR. Optimized single-slab three-dimensional spin-echo MR imaging of the brain. *Radiology*. 2000; 216:891–899. [PubMed: 10966728]
- Nash P, Wiley K, Brown J, Shinaman R, Ludlow D, Sawyer AM, Glover G, Mackey S. Functional magnetic resonance imaging identifies somatotopic organization of nociception in the human spinal cord. *Pain*. 2013; 154:776–781. [PubMed: 23618495]
- Nathan PW, Smith MC. Fasciculi proprii of the spinal cord in man. *Brain*. 1959; 82:610–668. [PubMed: 14426157]
- Petko M, Antal M. Propriospinal afferent and efferent connections of the lateral and medial areas of the dorsal horn (laminae I–IV) in the rat lumbar spinal cord. *J Comp Neurol*. 2000; 422:312–325. [PubMed: 10842234]

- Petko M, Veress G, Vereb G, Storm-Mathisen J, Antal M. Commissural propriospinal connections between the lateral aspects of laminae III–IV in the lumbar spinal cord of rats. *J Comp Neurol.* 2004; 480:364–377. [PubMed: 15558798]
- Pfeuffer J, van de Moortele PF, Yacoub E, Shmuel A, Adriany G, Andersen P, Merkle H, Garwood M, Ugurbil K, Hu X. Zoomed functional imaging in the human brain at 7 Tesla with simultaneous high spatial and high temporal resolution. *Neuroimage.* 2002; 17:272–286. [PubMed: 12482083]
- Pierrot-Deseilligny E, Marchand-Pauvert V. A cervical propriospinal system in man. *Adv Exp Med Biol.* 2002; 508:273–279. [PubMed: 12171122]
- Porszasz R, Beckmann N, Bruttel K, Urban L, Rudin M. Signal changes in the spinal cord of the rat after injection of formalin into the hindpaw: characterization using functional magnetic resonance imaging. *Proc Natl Acad Sci U S A.* 1997; 94:5034–5039. [PubMed: 9144185]
- Power JD, Barnes KA, Snyder AZ, Schlaggar BL, Petersen SE. Spurious but systematic correlations in functional connectivity MRI networks arise from subject motion. *Neuroimage.* 2012; 59:2142–2154. [PubMed: 22019881]
- Rieseberg S, Frahm J, Finsterbusch J. Two-dimensional spatially-selective RF excitation pulses in echo-planar imaging. *Magn Reson Med.* 2002; 47:1186–1193. [PubMed: 12111965]
- Seghier ML. Laterality index in functional MRI: methodological issues. *Magn Reson Imaging.* 2008; 26:594–601. [PubMed: 18158224]
- Smith SM, Jenkinson M, Woolrich MW, Beckmann CF, Behrens TE, Johansen-Berg H, Bannister PR, De Luca M, Drobnjak I, Flitney DE, Niazy RK, Saunders J, Vickers J, Zhang Y, De Stefano N, Brady JM, Matthews PM. Advances in functional and structural MR image analysis and implementation as FSL. *Neuroimage.* 2004; 23(Suppl 1):S208–219. [PubMed: 15501092]
- Soteropoulos DS, Edgley SA, Baker SN. Spinal commissural connections to motoneurons controlling the primate hand and wrist. *J Neurosci.* 2013; 33:9614–9625. [PubMed: 23739958]
- Sprenger C, Eippert F, Finsterbusch J, Bingel U, Rose M, Buchel C. Attention modulates spinal cord responses to pain. *Curr Biol.* 2012; 22:1019–1022. [PubMed: 22608507]
- Stroman PW, Wheeler-Kingshott C, Bacon M, Schwab JM, Bosma R, Brooks J, Cadotte D, Carlstedt T, Ciccarelli O, Cohen-Adad J, Curt A, Evangelou N, Fehlings MG, Filippi M, Kelley BJ, Kollias S, Mackay A, Porro CA, Smith S, Strittmatter SM, Summers P, Tracey I. The current state-of-the-art of spinal cord imaging: methods. *Neuroimage.* 2014; 84:1070–1081. [PubMed: 23685159]
- Sugiura Y, Lee CL, Perl ER. Central projections of identified, unmyelinated (C) afferent fibers innervating mammalian skin. *Science.* 1986; 234:358–361. [PubMed: 3764416]
- Summers PE, Ferraro D, Duzzi D, Lui F, Iannetti GD, Porro CA. A quantitative comparison of BOLD fMRI responses to noxious and innocuous stimuli in the human spinal cord. *Neuroimage.* 2010; 50:1408–1415. [PubMed: 20096788]
- van der Worp HB, Howells DW, Sena ES, Porritt MJ, Rewell S, O'Collins V, Macleod MR. Can animal models of disease reliably inform human studies? *PLoS Med.* 2010; 7:e1000245. [PubMed: 20361020]
- Wager TD, Atlas LY, Lindquist MA, Roy M, Woo CW, Kross E. An fMRI-based neurologic signature of physical pain. *N Engl J Med.* 2013; 368:1388–1397. [PubMed: 23574118]
- Weber, KA., II; Chen, Y.; Wang, X.; Parrish, TB. Choice of Motion Correction Method Affects Spinal Cord fMRI Results. 20th Annual Meeting of the Organization for Human Brain Mapping; Hamburg, Germany. 2014.
- Weber KA 2nd, Chen Y, Wang X, Kahnt T, Parrish TB. Lateralization of cervical spinal cord activity during an isometric upper extremity motor task with functional magnetic resonance imaging. *Neuroimage.* 2016; 125:233–243. [PubMed: 26488256]
- Wheeler-Kingshott CA, Stroman PW, Schwab JM, Bacon M, Bosma R, Brooks J, Cadotte DW, Carlstedt T, Ciccarelli O, Cohen-Adad J, Curt A, Evangelou N, Fehlings MG, Filippi M, Kelley BJ, Kollias S, Mackay A, Porro CA, Smith S, Strittmatter SM, Summers P, Thompson AJ, Tracey I. The current state-of-the-art of spinal cord imaging: applications. *Neuroimage.* 2014; 84:1082–1093. [PubMed: 23859923]
- Willis WD, Kenshalo DR Jr, Leonard RB. The cells of origin of the primate spinothalamic tract. *J Comp Neurol.* 1979; 188:543–573. [PubMed: 118192]

- Willis WD, Westlund KN. Neuroanatomy of the pain system and of the pathways that modulate pain. *J Clin Neurophysiol.* 1997; 14:2–31. [PubMed: 9013357]
- Woolf CJ. Evidence for a central component of post-injury pain hypersensitivity. *Nature.* 1983; 306:686–688. [PubMed: 6656869]
- Woolrich M. Robust group analysis using outlier inference. *Neuroimage.* 2008; 41:286–301. [PubMed: 18407525]
- Woolrich MW, Behrens TE, Beckmann CF, Jenkinson M, Smith SM. Multilevel linear modelling for FMRI group analysis using Bayesian inference. *Neuroimage.* 2004; 21:1732–1747. [PubMed: 15050594]
- Woolrich MW, Ripley BD, Brady M, Smith SM. Temporal autocorrelation in univariate linear modeling of FMRI data. *Neuroimage.* 2001; 14:1370–1386. [PubMed: 11707093]
- Worsley, KJ. Statistical analysis of activation images. In: Jezzard, P.; Matthews, PM.; Smith, SM., editors. *Functional MRI: An Introduction to Methods.* Oxford University Press; USA: 2001.
- Yang JF, Gorassini M. Spinal and brain control of human walking: implications for retraining of walking. *Neuroscientist.* 2006; 12:379–389. [PubMed: 16957000]
- Yang PF, Wang F, Chen LM. Differential fMRI Activation Patterns to Noxious Heat and Tactile Stimuli in the Primate Spinal Cord. *J Neurosci.* 2015; 35:10493–10502. [PubMed: 26203144]
- Zhao F, Williams M, Welsh DC, Meng X, Ritter A, Abbadie C, Cook JJ, Reicin AS, Hargreaves R, Williams DS. fMRI investigation of the effect of local and systemic lidocaine on noxious electrical stimulation-induced activation in spinal cord. *Pain.* 2009; 145:110–119. [PubMed: 19560271]

Highlights

- fMRI was used to detect sensory activity in the cervical spinal cord
- Warm and painful thermal stimuli were applied to the ventral right forearm
- The activity was localized to the dorsal hemicord at the group and subject level
- The spatial extent and magnitude of the activity was greater for painful stimuli
- A machine-learning algorithm decoded the stimuli based on the pattern of activity

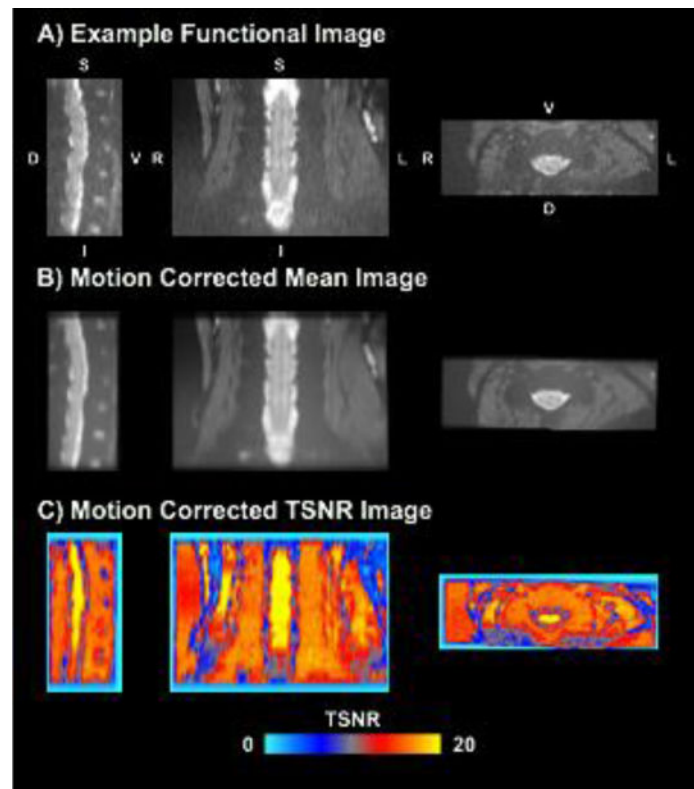
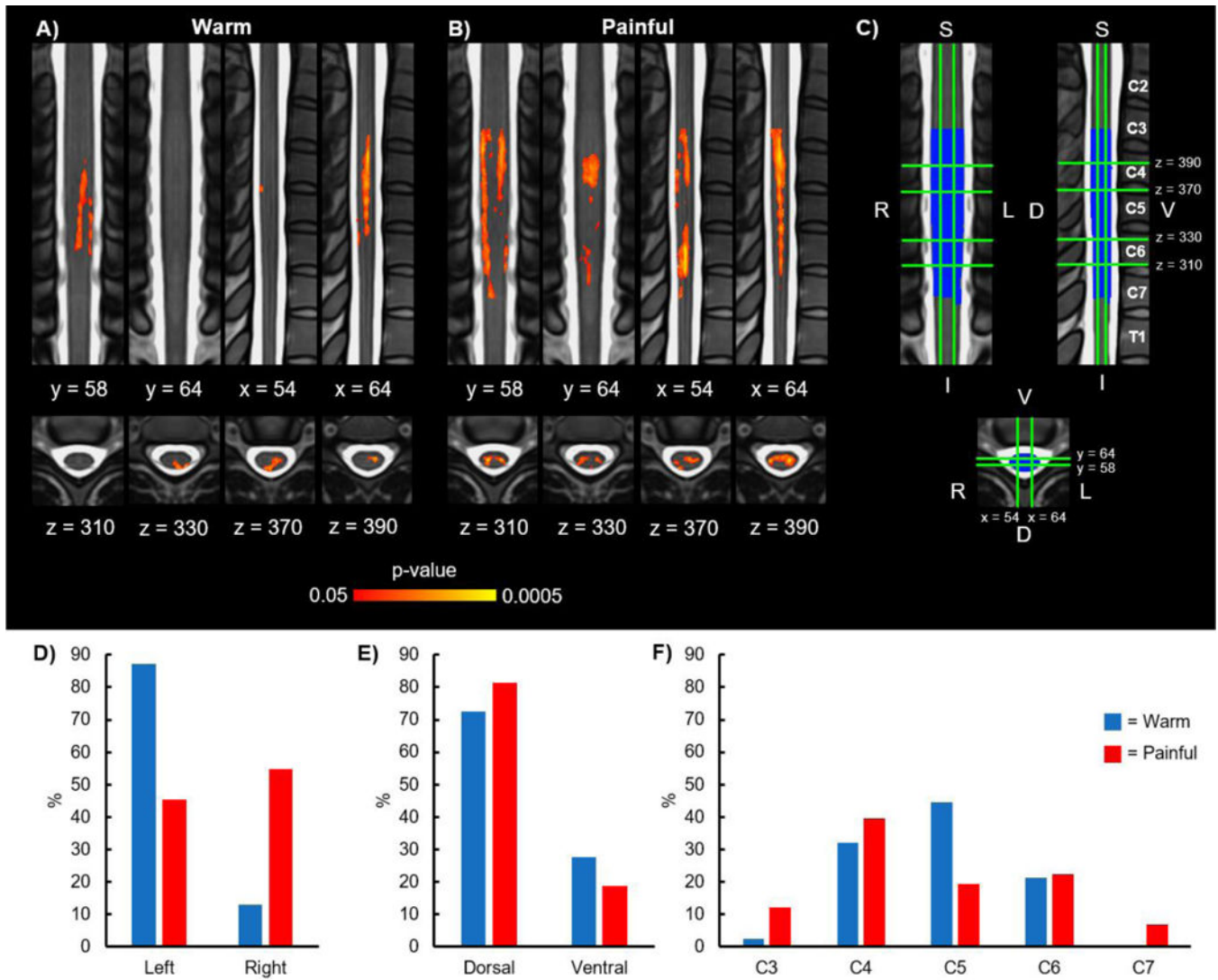


Figure 1. An example functional image (A), motion corrected mean image (B), and motion corrected temporal signal to noise ratio (TSNR) image (C) are shown. The images were generated from a randomly selected subject. L = left, R = right, D = dorsal, V = ventral, S = superior, I = inferior.

**Figure 2.**

Group activity for the warm and painful stimuli. A) Group average activation maps (2 coronal, 2 sagittal, and 4 axial slices) for the warm stimulus. B) Group average activation maps (2 coronal, 2 sagittal, and 4 axial slices) for the painful stimulus. C) Legend showing orientation and location of the coronal ($y = 58$ and $y = 64$), sagittal ($x = 54$ and $x = 64$), and axial ($z = 310$, $z = 330$, $z = 370$, and $z = 390$) slices on the MNI-Poly-AMU spinal cord template with the corresponding vertebrae labeled. The location of the slices remains constant across all of the figures. The group mask generated from the intersection of the subject level functional images is shown in blue. D) Location of the group average activity shown in A and B in the left and right hemicords. E) Location of the group average activity shown in A and B in the dorsal and ventral hemicords. F) Location of the group average activity shown in A and B at the C3, C4, C5, C6, and C7 vertebral levels. The activation maps were thresholded at a $p < 0.05$ with a cluster-level corrected threshold of $p < 0.05$. The background image is the MNI-Poly-AMU spinal cord template. % = percentage of the active

voxels located in the corresponding hemicord or vertebral level. L = left, R = right, D = dorsal, V = ventral, S = superior, I = inferior.

Author Manuscript

Author Manuscript

Author Manuscript

Author Manuscript

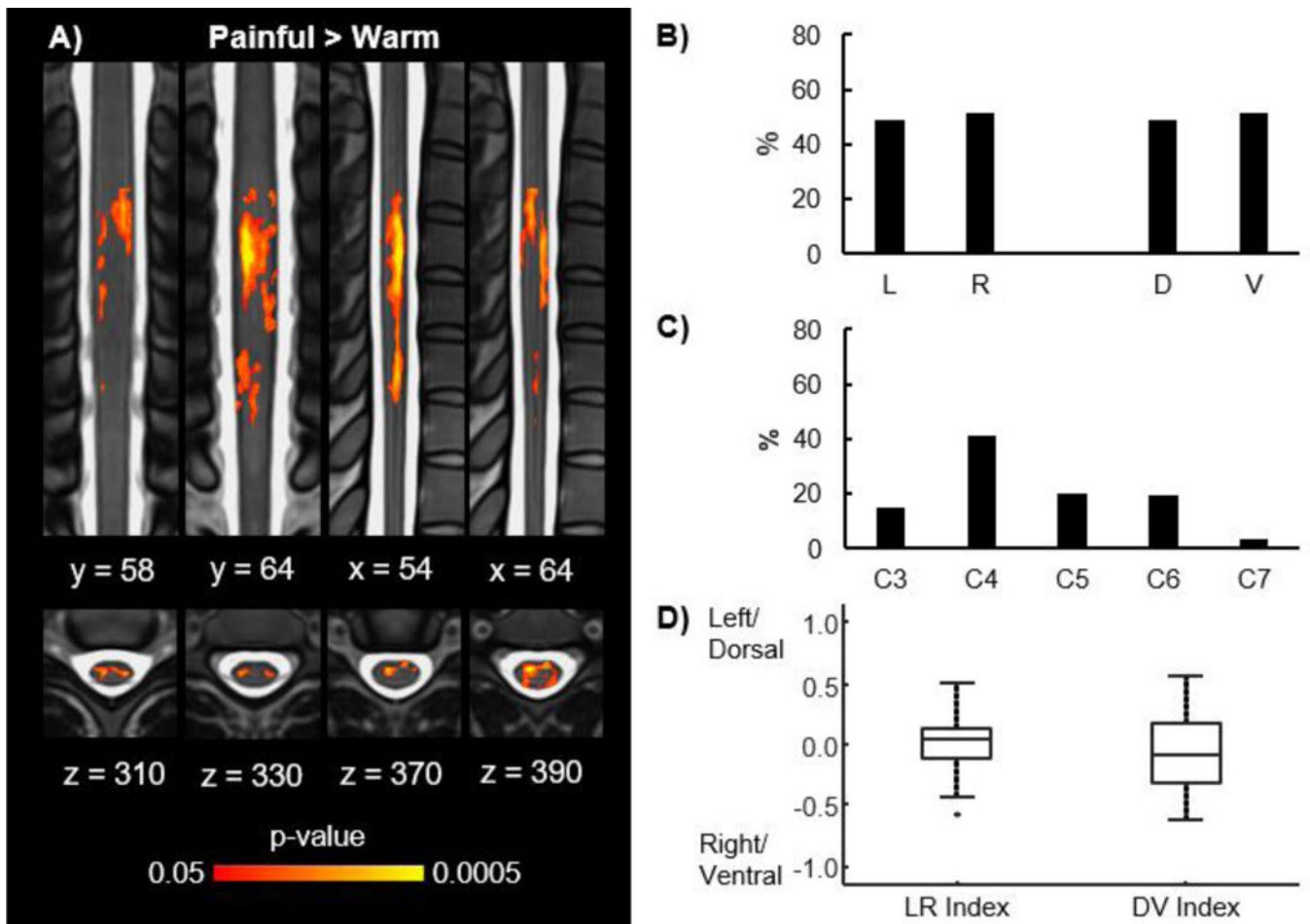


Figure 3.

Group activity for the painful > warm contrast. A) Group average activation maps (2 coronal, 2 sagittal, and 4 axial slices) for the painful > warm contrast. B) Location of the group average activity shown in A in the left (L), right (R), dorsal (D), and ventral (V) hemicords. C) Location of the group average activity shown in A at the C3, C4, C5, C6, and C7 vertebral levels. D) Box plots showing the distribution of the left-right (LR) and dorsal-ventral (DV) indices across the subjects for the painful > warm contrast. No significant localization of the activity to any hemicord was present across the subjects. The activation maps were thresholded at a $p < 0.05$ with a cluster-level corrected threshold of $p < 0.05$. Refer to Figure 2C for the legend showing the orientation and location of the slices on the MNI-Poly-AMU spinal cord template. % = percentage of the active voxels located in the corresponding hemicord or vertebral level.

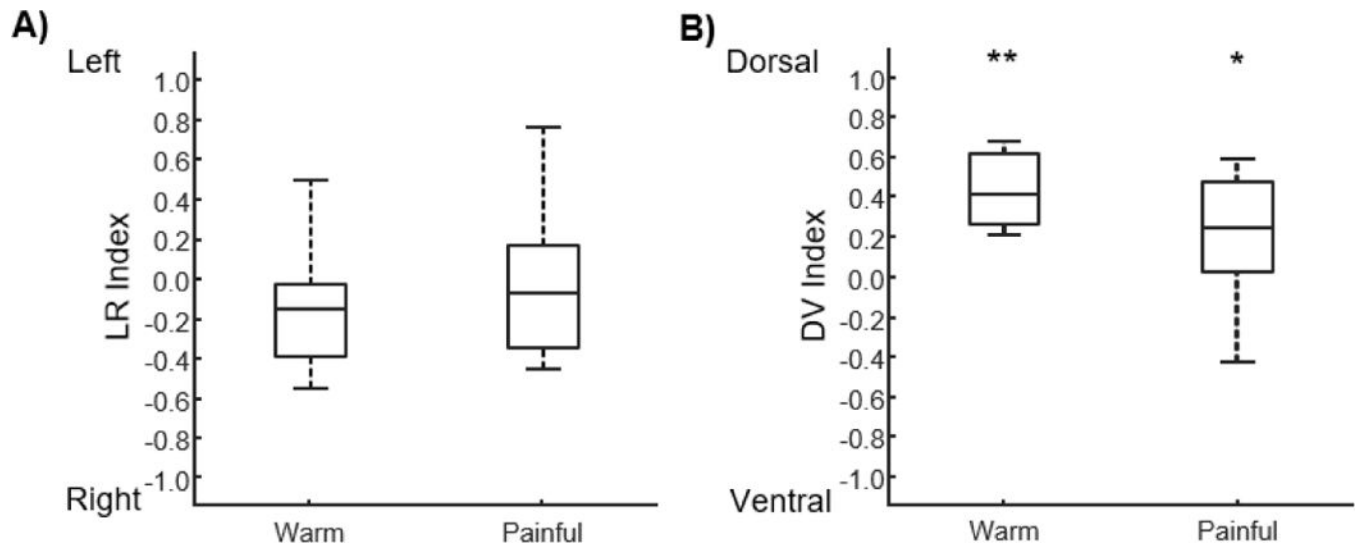


Figure 4.

Box plots showing the distribution of the left-right (LR) and dorsal-ventral (DV) indices across the subjects for the warm and painful stimuli. A) No significant localization of the activity to the left or right hemicord was present for either stimulus. B) For both stimuli, the activity was significantly localized to the dorsal hemicord. * $p < 0.05$, ** $p < 0.01$.

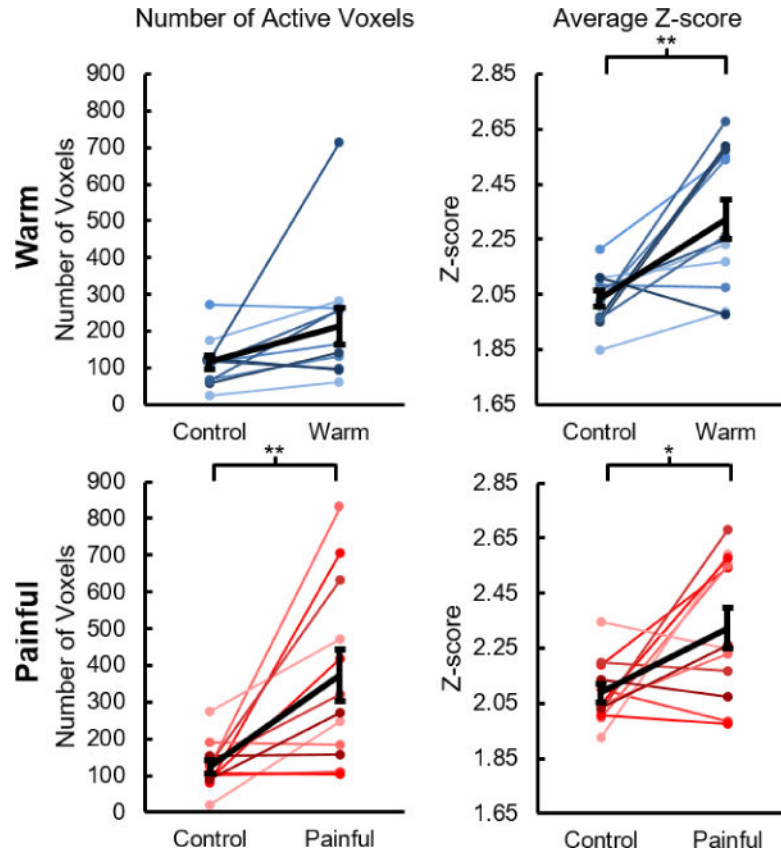


Figure 5. Number of active voxels and average Z-score of the active voxels for thermal stimulation compared to the control analysis. At the subject level, the number of active voxels for thermal stimulation tended to be greater than the control analysis for the warm stimulus but was not significantly greater. For the painful stimulus, the number of active voxels for thermal stimulation was significantly greater than the control analysis. For both the warm and painful stimuli, the average Z-score of the active voxels for thermal stimulation was significantly greater than the control analysis. At the group level, no activity was present for the control analysis. The average number of active voxels and the average Z-score of the active voxels across the subjects are shown in black. Error bars = \pm one standard error. * $p < 0.05$ and ** $p < 0.01$.

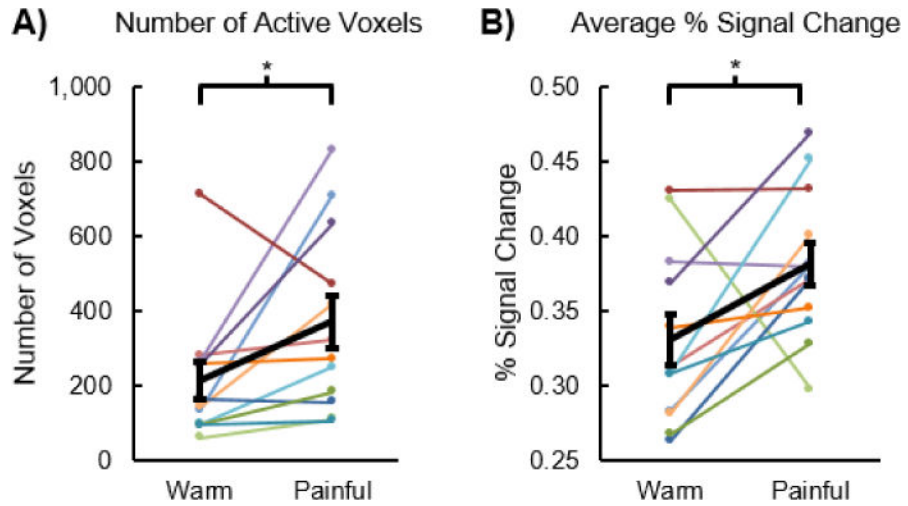


Figure 6. Number of active voxels and signal change for the warm stimulus compared to the painful stimulus. A) The number of active voxels was significantly greater for the painful stimulus than the warm stimulus. B) The average percent signal change for the warm and painful stimuli was also significantly greater for the painful stimulus than the warm stimulus. The average percent signal change was calculated using the subject level activation maps generated from the average of the six runs. Average in black. Error bars = \pm one standard error. * $p < 0.05$.

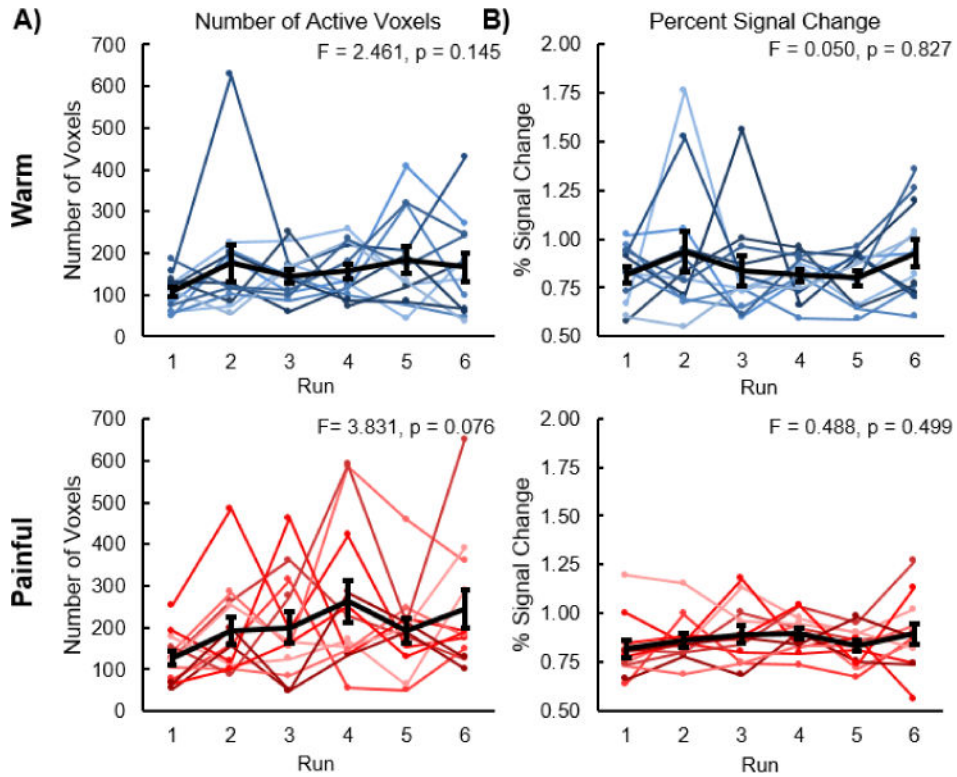


Figure 7.

Number of active voxels and percent signal change of the active voxels across the subjects for each of the six runs. A) No linear increase or decrease in the number of active voxels was present for the warm stimulus. The number of active voxels tended to linearly increase for the painful stimulus, but this trend was not significant. B) No linear increase or decrease in the percent signal change of the active voxels was present for either the warm or painful stimuli. The average number of active voxels and the average percent signal change of the active voxels across the subjects are shown in black. The average percent signal change was calculated using the subject level activation maps generated from each run. Error bars = \pm one standard error.

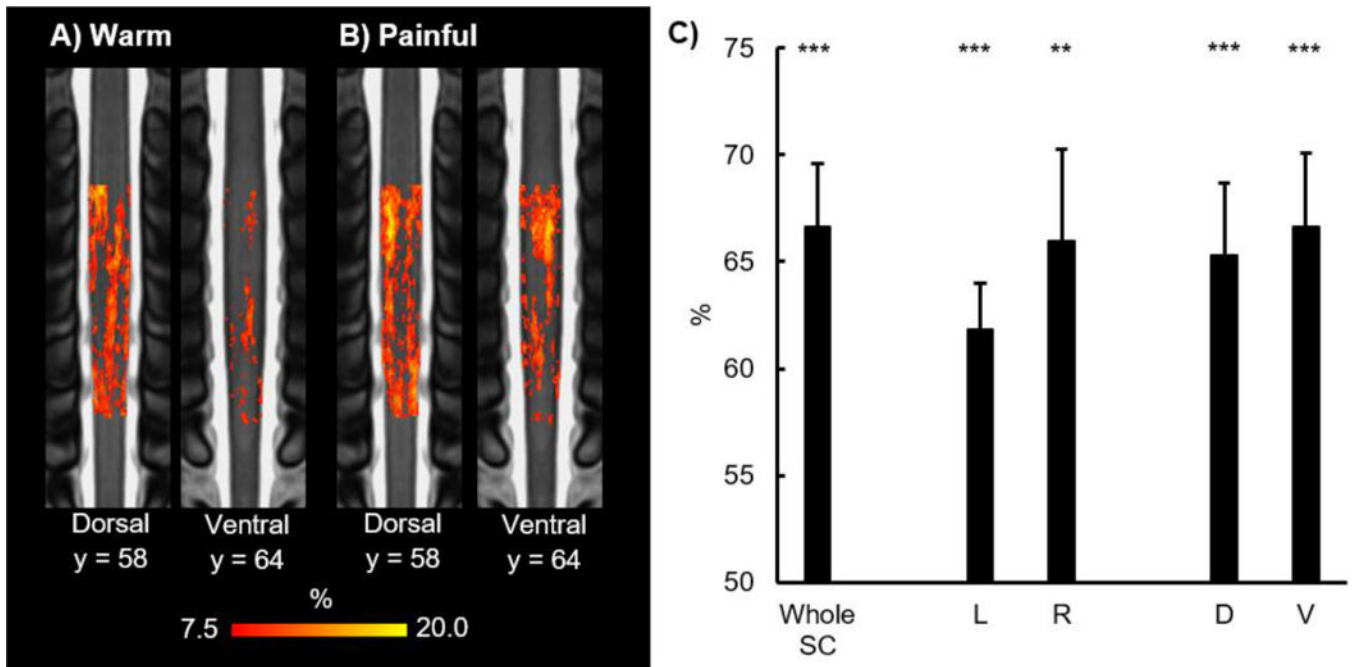


Figure 8.

Results of the run-wise multi-voxel pattern analysis (MVPA) are shown. Across subject run-wise contingency maps for the warm (A) and painful (B) stimuli are shown (2 coronal slices). The consistency maps show the percentage across all runs and all subjects that a voxel was active. C) Percent accuracy of the run-wise MVPA across the whole spinal cord (SC) and within the left (L), right (R), dorsal (D), and ventral (V) hemicords is shown. MVPA was able to successfully decode the warm and painful stimuli better than chance across the whole spinal cord and within each hemicord. Refer to Figure 2C for the legend showing the orientation and location of the slices on the MNI-Poly-AMU spinal cord template. Error bars = \pm one standard error. ** $p < 0.01$ and *** $p < 0.001$.

Table 1

Summary of Group Activity

Contrast	Number of Active Voxels	Average Z-Score	Maximum Z-Score	Coordinates			Center-of-Gravity		
				x	y	z	x	y	z
Warm	3,978	2.126	3.125	64	62	398	62.5	58.3	359.0
Painful	11,428	2.146	3.432	65	60	395	58.4	59.7	364.0
Painful > Warm	9,394	2.185	4.171	55	63	382	59.4	61.3	370.0